Backbone Dynamics and Structural Characterization of the Partially Folded A State of Ubiquitin by ^{1}H, ^{13}C, and ^{15}N Nuclear Magnetic Resonance Spectroscopy†

Bernhard Brutscher, Rafael Brüschweiler, and Richard R. Ernst*

Laboratorium für Physikalische Chemie, Eidgenössische Technische Hochschule Zentrum, 8092 Zürich, Switzerland

Received June 25, 1997; Revised Manuscript Received August 11, 1997⊗

ABSTRACT: Structure and dynamics of the partially folded A state of ubiquitin in a 60%/40% methanol/water mixture at pH 2 was studied by two- and three-dimensional nuclear magnetic resonance spectroscopy (NMR) using fully ^{13}C,^{15}N-labeled ubiquitin. Complete backbone ^{13}CO, $^{13}C^{\alpha}$, ^{15}N, and $^{1}H^{N}$ assignment was achieved. ^{13}CO and $^{13}C^{\alpha}$ chemical shifts and $^{1}H-^{1}H$ nuclear Overhauser enhancement (NOE) connectivities indicate different behavior for the N-terminal and the C-terminal halves of the protein. In the N-terminal half of the A state, comprising the antiparallel β-sheet and the central α-helix, the native secondary structural elements are largely conserved. The C-terminal half, which is in the native form rich in β-strand character, undergoes a methanol-induced transition to a dynamic state with a uniformly high propensity for helical structure. This behavior is also reflected in backbone ^{15}N relaxation data, indicating the presence of three loosely coupled secondary structural segments with enhanced internal mobility as compared to the native state.

Partially folded states exist for a number of proteins under nonnative conditions, such as low pH and high concentrations of alcohol, urea, or guanidine hydrochloride. Under these conditions, tertiary protein interactions are often weakened and the conformational propensities are dominated by short-range interactions within the polypeptide chain. The investigation of the residual structure in partially or fully denatured proteins may provide insights into the interactions responsible for their formation as well as their possible role in the early stages of protein folding. Studies by liquid-state nuclear magnetic resonance (NMR)[1] have been performed on partially denatured proteins (Buck *et al.*, 1995; Frank *et al.*, 1995; Redfield *et al.*, 1994; Feng *et al.*, 1994; Alexandrescu *et al.*, 1994 a,b; Logan *et al.*, 1994; van Mierlo *et al.*, 1993; Neri *et al.*, 1992) to determine regions of well-defined residual structure.

Equally important is the detailed characterization of the dynamics of these states as there is evidence that they are highly mobile. NMR relaxation measurements of ^{15}N or ^{13}C nuclei allow one to study local molecular motions on pico- to microseconds time scales. While this methodology [for a review see Tycko (1994)] is now widely applied to native states of globular proteins, so far only a few studies have been reported on partially denatured proteins (Farrow *et al.*, 1995, 1997; Alexandrescu & Shortle, 1994; Buck *et al.*, 1996; Frank *et al.*, 1995). The high degree of internal motion found for the nonnative states justifies detailed motional studies and the development of advanced motional models to further elucidate the relationship between residual structure and molecular flexibility.

Ubiquitin is a small globular protein of 76 amino acids (molecular mass of 8.6 kDa), which contains neither prosthetic groups nor disulfide bridges. Ubiquitin is found in all eukaryotes and it is involved in a variety of biochemical functions, including protein degradation and differential gene regulation [for a review, see Rechsteiner *et al.* (1988)]. The native form of ubiquitin has been characterized structurally by X-ray crystallography (Vijay-Kumar *et al.*, 1987) and NMR (Di Stefano & Wand, 1987; Weber *et al.*, 1987) and dynamically by NMR relaxation (Schneider *et al.*, 1992; Tjandra *et al.*, 1995). The native structure shows a high content of secondary structural elements (five-stranded β-sheet, α-helix, 3_{10}-helix, and 7 reverse turns). While little is known about the structural and dynamical details of the ubiquitin function, there is evidence that it requires conformational flexibility: Incorporation of a disulfide bridge between residues 4 and 66 leads to a 70−80% decrease of activity in signaling proteolysis, which suggests that biological functions of ubiquitin involve large-scale intramolecular motions (Ecker *et al.*, 1989).

Since under ambient conditions ubiquitin is remarkably stable with an unusually rigid backbone structure as shown by NMR relaxation (Schneider *et al.*, 1992; Tjandra *et al.*, 1995), it is interesting to study ubiquitin under conditions that destabilize the native structure to learn more about the behavior of the secondary structural elements with respect to changes in the solvent environment. Such work was initiated by Wilkinson and Mayer (1986), who investigated ubiquitin by circular dichroism (CD) in different solvents as a function of the dielectric constant, and they found that in water/alcohol mixtures at room temperature and low pH ($\cong$2), a partially folded state of ubiquitin is stabilized, which is called the *A* state of ubiquitin. In subsequent studies this state was further characterized by quenched hydrogen exchange measurements (Pan & Briggs, 1992), ^{1}H NMR

† This project has been supported by the Swiss National Science Foundation. B.B. is recipient of an EMBO fellowship.

* To whom correspondence should be addressed.

⊗ Abstract published in *Advance ACS Abstracts,* October 1, 1997.

[1] Abbreviations: NMR, nuclear magnetic resonance; CD, circular dichroism; MD, molecular dynamics; WATERGATE, water suppression by gradient-tailored excitation; TPPI, time-proportional phase incrementation; NOESY, nuclear Overhauser enhancement spectroscopy; HMQC, heteronuclear multiple-quantum spectroscopy; NOE, nuclear Overhauser effect; HSQC, heteronuclear single-quantum spectroscopy; CSA, chemical shielding anisotropy; DD, dipolar interaction; CSI, chemical shift index; TFE, trifluoroethanol.

S0006-2960(97)01538-9 CCC: $14.00

(Harding *et al*., 1991; Woolfson *et al.*, 1991 and 1993), ^{15}N-edited ^{1}H NMR (Stockman *et al*., 1993), CD (Cox *et al.* 1993), and molecular dynamics (MD) computer simulations (Alonso & Daggett, 1995).

These studies led in part to contradictory conclusions. Most authors agree that the N-terminal half remains nativelike, whereas diverging conclusions were reached about the average structure of the C-terminal half. While in the original CD work (Wilkinson & Mayer, 1986) a strong increase of helicity of the A state was observed, early NMR work concluded that the C-terminal half remained to a good extent nativelike (Harding *et al*., 1991; Woolfson *et al.*, 1991; Pan & Briggs, 1992). However, a ^{15}N-edited ^{1}H NMR study (Stockman *et al*., 1993) and a CD reinvestigation of the A state (Cox *et al.*, 1993) lend support to the original CD observations of Wilkinson and Mayer that the C-terminal half adopts a state with a high helical propensity. The MD simulations, on the other hand, showed nonnative behavior for the C-terminal half without an increase in helicity (Alonso & Daggett, 1995).

Here we report an investigation of the structure and main-chain dynamics of the A state of ubiquitin using isotopic ^{13}C,^{15}N-labeling and multidimensional NMR at three magnetic field strengths (400, 600, and 800 MHz ^{1}H frequency). The model emerging from ^{13}C chemical shifts, ^{1}H$-^{1}$H NOEs, and ^{15}N relaxation data consists of three distinct secondary structural elements: an antiparallel β-sheet and two helices, forming rather independent motional units. The N-terminal β-sheet and the central α-helix (helix *B*) remain nativelike, whereas the C-terminal part (residues 39−72) undergoes under the influence of methanol a transition from a β-sheet to a structure with predominant helical character (helix *A*). The backbone dynamics can be rationalized in terms of residue-specific effective tumbling correlation times, order parameters, and internal correlation times using an approach similar to the extended model-free approach (Clore *et al.*, 1990). The emerging picture is qualitatively consistent with the CD results (Wilkinson & Mayer, 1986; Cox *et al.*, 1993) and substantially refines the model by Stockman *et al.* (1993).

MATERIALS AND METHODS

Sample Preparation. ^{13}C,^{15}N-labeled ubiquitin was kindly provided by A. J. Wand (Buffalo, NY) and purchased from VLI (Southeastern, PA). A protocol for gene construction and protein expression in minimal medium was described by Wand *et al.* (1996). NMR samples of the A state of ubiquitin were prepared by dissolving 1−3 mg of ^{13}C,^{15}N-labeled ubiquitin in 200 μL of H_2O and 300 μL of CD_3OH (purchased from Cambridge Isotope Laboratories), resulting in concentrations of 0.2−0.7 mM. The pH was then adjusted to 2.0 by adding HCl and the samples were kept in sealed standard 5 mm NMR tubes. Samples with higher protein concentrations showed gelation several weeks after sample preparation and were not used for analysis. In the chosen concentration range (0.2−0.7 mM) the A-state samples remained liquid and transparent for at least 6 months. To optimize reliability, all relaxation measurements were performed on freshly prepared samples (not older than 1 week).

NMR Experiments. NMR experiments were performed on a Bruker AMX-600 spectrometer equipped with a triple-resonance (^{1}H, ^{15}N, ^{13}C) probe including shielded z gradients. Additional ^{15}N relaxation experiments were recorded on Bruker DMX-400 and DMX-800 spectrometers, both with triple-resonance (^{1}H,^{13}C,^{15}N) equipment and triple-axis gradients. The sample temperature was set to 300 K. For all NMR experiments, WATERGATE (Sklenar *et al.*, 1993) and water flip-back pulses (Grzesiek *et al.*, 1993) were inserted in the pulse sequences to obtain a relaxed spin state for the water magnetization before acquisition. Pulsed-field *z* gradients were applied for coherence-transfer-pathway selection (Bax & Pochapsky, 1992). Quadrature detection in the indirect dimensions of the multidimensional experiments was obtained by the TPPI-States method (Marion *et al.*, 1989). The spectral widths and the carrier frequencies (in parentheses) were set for ^{1}H to 10 ppm (4.76 ppm), for ^{15}N to 19 ppm (118.76 ppm), for $^{13}C^{\alpha}$ to 15 ppm (57.2 ppm), for ^{13}CO to 10 ppm (173.9 ppm), and for aliphatic ^{13}C to 60 ppm (42.6 ppm). The frequency was switched on the ^{13}C channel by time-proportional phase incrementation during radiofrequency (rf) pulses. Data processing and peak picking were performed using the FELIX program version 95.0 (Biosym Technologies).

Three-dimensional MQ-HNCOCA and 3D HNCA (*Brutscher et al., 1995; Grzesiek et al., 1992) correlation experiments* were carried out at 600 MHz ^{1}H frequency for chemical shift assignment of the backbone nuclei H^N, N, CO, and C^{α}. A 3D MQ-HNCOCA data set was acquired with 512 (^{1}H) × 160 (^{13}C) × 40 (^{15}N) complex points and 4 scans per (t_1, t_2) increment resulting in an experimental time of 40 h. The C^{α} and CO frequency evolution is encoded in the same indirect dimension of the 3D spectrum. A pair of cross peaks is detected for each H^N_i, N_i, CO_{i-1}, C^{α}_{i-1} correlation with the CO chemical shift given by the center frequency and the C^{α} chemical shift defined by their separation. The scaling factor between CO and C^{α} chemical shift evolution was set to $\lambda = 2.0$. The spectral width in the ^{13}C dimension was set to 33 ppm and the effective demodulation frequency of the C^{α} was shifted to 67 ppm (Brutscher *et al.*, 1995). A 3D HNCA data set was acquired with 512 (^{1}H) × 40 (^{13}C) × 40 (^{15}N) complex data points and 16 scans per (t_1, t_2) increment, resulting in a total measurement time of 40 h. The data were zero-filled and Fourier-transformed to final 3D spectra with 512 × 256 × 256 data points.

Three-dimensional ^{13}C/^{15}N and ^{15}N/^{15}N doubly edited ^{1}H−^{1}H NOESY experiments were performed at 600 MHz ^{1}H frequency for the structural characterization of the protein. The pulse sequences were derived from a standard ^{1}H$-^{1}$H NOESY experiment (Jeener *et al.*, 1979) by adding ^{1}H$-^{13}$C HMQC (Bax *et al*., 1983) and ^{1}H$-^{15}$N HSQC (Bodenhausen & Ruben, 1980) pulse-sequence blocks before and after the NOESY mixing period. (C, N, H^N) and (N, N,H^N) data sets were acquired with 94 × 60 × 512 and 78 × 78 × 512 complex points, respectively. Eight scans per (t_1, t_2) increment resulted in an experimental time of 4 days per experiment. The data were zero-filled and transformed to final 3D spectra of 256 × 256 × 512 data points.

Two-dimensional ^{12}C/^{14}N and ^{13}C/^{15}N-filtered ^{1}H−^{1}H NOESY experiments were done at 600 MHz ^{1}H frequency on a sample containing a mixture of 50% unlabeled and 50% ^{13}C,^{15}N-labeled ubiquitin under the aforementioned A-state sample conditions. The pulse sequence includes double-tuned ^{13}C/^{15}N isotope filters before and after the NOESY mixing period (Burgering *et al.*, 1993) and is provided as supporting information. The total acquisition time for 256

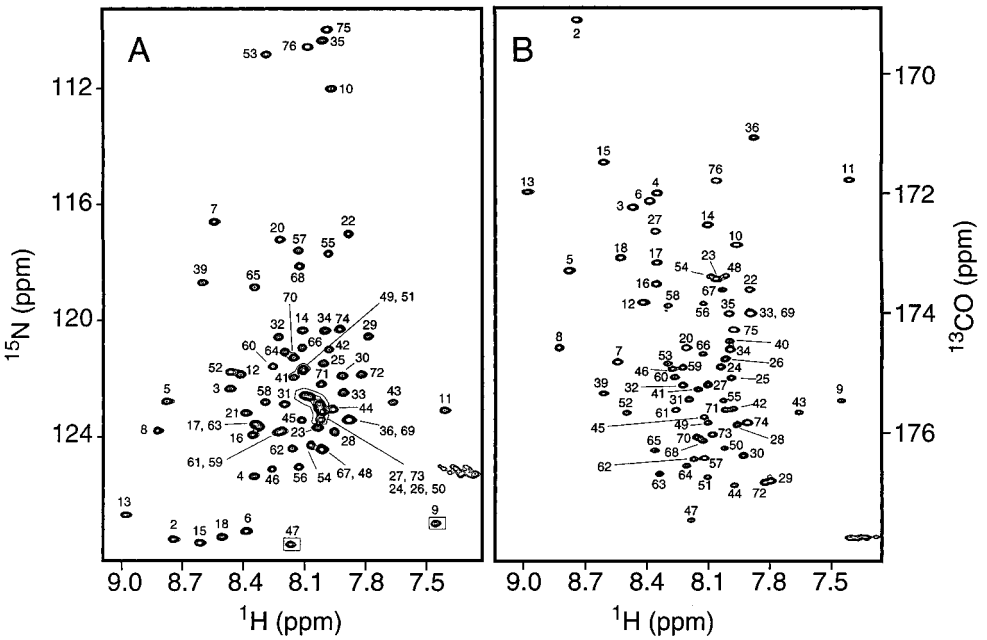

FIGURE 1: Two-dimensional $^{1}H^{N}-^{15}N$ (A) and $^{1}H^{N}-^{13}CO$ (B) correlation spectra of the ubiquitin A state recorded at 600 MHz ^{1}H frequency. Residue numbers (of the amide protons) are given for all 72 cross peaks. The ^{15}N frequencies of residues 9 and 47 (A) are outside the chosen spectral width, and the corresponding cross peaks are folded back into the displayed spectrum.

$\times$ 1024 complex data points was 70 h. Data sets recorded with different pulse phases were combined to yield separate intra- and intermolecular NOESY spectra.

Two-dimensional ^{15}N relaxation experiments (T_1, T_2, NOE) were performed on doubly ^{13}C,^{15}N-labeled samples of ubiquitin A state at 400, 600, and 800 MHz ^{1}H frequency. The pulse sequences used are similar to those proposed by others [see for example Peng and Wagner (1992); Farrow *et al.*, 1994] and are provided as supporting information. Since doubly ^{13}C,^{15}N-labeled samples of ubiquitin were used, the C^{α} and CO nuclei had to be broadband-decoupled during t_1, and selective C^{α} and CO 180° pulses were applied during the T_1 and T_2 relaxation delays to suppress effects caused by cross-correlation between ^{15}N chemical shielding anisotropy (CSA) and $^{15}N-^{13}C$ dipolar (DD) interactions. During the T_2 relaxation period, chemical shift and J_{NH}-coupling evolution was suppressed by applying a spin-lock field of $|\gamma_N B_1|/2\pi = 2.5$ kHz. In these experiments the magnetization is locked along an effective field vector with an orientation depending on the frequency offset $\Delta\nu$ of the ^{15}N nucleus. The measured relaxation rates T_2^{meas} were corrected for these offset effects using the relation $T_2^{corr} = T_2^{meas}(T_1 \sin^2\theta)/(T_1 - T_2^{meas}\cos^2\theta)$ with $\tan\theta = |\gamma_N B_1|/2\pi\Delta\nu$. The temperature dependence of differential cross-peak shifts in the $^{1}H-^{15}N$ correlation spectrum was used as an internal probe for calibration of the actual sample temperature. In this way, it was assured that the sample temperature variation between the different relaxation experiments is less than 0.4 K. The T_1 relaxation decay was sampled at eight time points: 20, 120, 240, 380, 460, 560, 760, and 1000 ms at 400 and 600 MHz and 20, 120, 240, 380, 540, 720, 1000, and 1500 ms at 800 MHz. The T_2 relaxation decay was sampled at nine different time points: 8, 24, 48, 72, 96, 120, 160, 200, and 280 ms at 400 and 600 MHz. The total data collection time for each series of T_1 and T_2 was 12 h (at 800 MHz), 19 h (at 600 MHz), and 46 h (at 400 MHz). For the $\{^{1}H\}^{15}N$-NOE measurements, two spectra with ^{1}H saturation and one without were recorded in an interleaved manner. Different ^{1}H saturation schemes were used during the recycle delay of 3.5 s: either a windowless WALTZ-16 sequence or a train of 120° pulses applied every 10 ms. The total experimental time per experiment was 72 h (at 600 MHz) and 36 h (at 800 MHz).

Analysis of ^{15}N Relaxation Data. All data sets of a relaxation series were processed identically. The time-domain data were multiplied with a 30°-shifted squared cosine function for resolution enhancement (Figure 1). Peak intensities were extracted from 2D spectra with high digital resolution (^{1}H, 2.3 Hz; ^{15}N, 1.5 Hz) using a local grid search routine for each cross peak. T_1 and T_2 values were determined by fitting the measured peak heights to a two-parameter function of the form

$$I(T) = I_0 \exp(-T/T_{1,2}) \qquad (1)$$

where $I(T)$ is the intensity after a delay time T and I_0 is the intensity at $T = 0$. The steady-state NOE values were determined from the ratios of the measured cross-peak intensities in the presence (I_{sat}) and absence (I_{unsat}) of ^{1}H saturation:

$$NOE^{meas} = I_{sat}/I_{unsat} \qquad (2)$$

No systematic deviation was found for the different saturation schemes used. To estimate the systematic errors in the measured NOE^{meas} due to the finite recycle delay of $\tau_R = 3.5$ s, the H^N T_1 relaxation times were measured for the A state of ubiquitin at 600 MHz. T_1 values are found between 450 and 730 ms with a mean value and standard deviation of 605 $\pm$ 60 ms. Assuming steady-state conditions, the correction of the measured NOE values for the finite saturation time (Skelton *et al.*, 1993) was less than 0.02.

The relaxation measurements at 600 MHz field strength were repeated several times (four T_1 sets, four T_2 sets, and three complete NOE sets) using freshly prepared ubiquitin

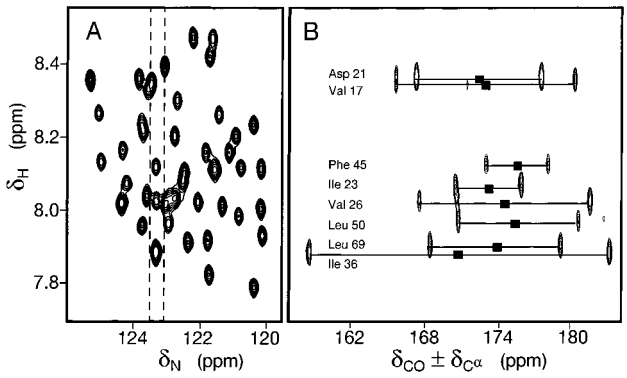

FIGURE 2: Backbone resonance assignment (H^N, N, CO, C^α) of the ubiquitin A state. Panel A shows the most crowded region of the $^1H-^{15}N$ correlation spectrum in Figure 1A. Overlapping cross peaks are resolved by the corresponding ^{13}CO and $^{13}C^\alpha$ frequencies. Panel B shows a plane of the 3D MQ-HNCOCA triple resonance spectrum taken at the ^{15}N frequency indicated by a bar in panel A. The ^{13}CO chemical shifts are obtained from the center positions of peak pairs, whereas the separation of the two peaks, $\Delta\delta$, determines the $^{13}C^\alpha$ chemical shift δ_{C^α} according to the relation $\delta_{C^\alpha}(ppm) = 67\ ppm - \Delta\delta(ppm)$.

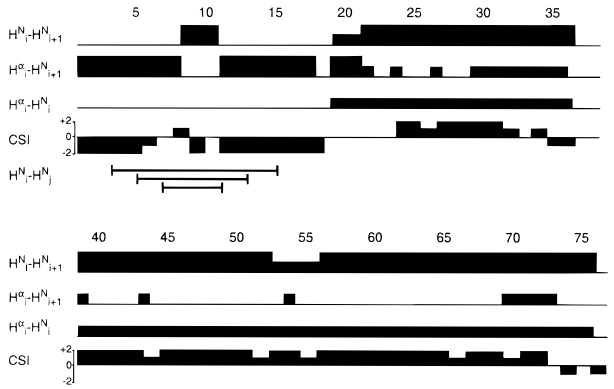

FIGURE 3: Short- and medium-range $^1H-^1H$ NOEs of the ubiquitin A state as identified from $^{15}N/^{15}N$- and $^{13}C/^{15}N$-filtered NOESY experiments. The intensities are classified as strong, weak, or absent, taking into account different line widths for the different segments of the protein. The ^{13}C chemical shift information is plotted in terms of the chemical shift index (CSI) of Wishart and Sykes (1994). Positive CSI values within a segment of the polypeptide sequence indicate the preference of helical conformation; negative values are typical for β-sheet structures.

samples to estimate systematic and statistical errors in the experimental data.

RESULTS AND DISCUSSION

Backbone Assignment. A general feature of partially denatured proteins is the reduction of the ^1H chemical shift range as compared to their native form. In the A state of ubiquitin, 88% of the amide protons resonate within a frequency range of 0.8 ppm (7.8−8.6 ppm) as shown in Figure 1A, while in the native state of ubiquitin the resonances are almost uniformly dispersed over a range of 2.5 ppm. Therefore, the standard approach for resonance assignment by ^1H NMR fails for the A state. Fortunately, the frequency dispersion of the ^{13}C and ^{15}N resonances is only little influenced by the tertiary structure of the protein. Panels A and B of Figure 1 show the dispersion of the ^{15}N and ^{13}CO backbone resonances of ubiquitin in the A state. The use of triple-resonance multidimensional NMR techniques (Ikura *et al*., 1990; Kay *et al*., 1990; Montelione & Wagner, 1990) offers a straightforward way for resonance assignment of partially or totally denatured protein states. In our case, the 3D MQ-HNCOCA experiment was used to resolve overlapping $^1H-^{15}N$ HSQC correlations by their different CO and C^α chemical shifts. Figure 2B shows a plane of the 3D MQ-HNCOCA spectrum taken at a ^{15}N frequency of 123.3 ppm (indicated by a gray bar in Figure 2A). The overlapping $^1H-^{15}N$ cross peaks are now easily identified by the separate two-peak patterns in the ^{13}C dimension (for example, in the case of the overlapping residues 36 and 69) and the CO and C^α frequencies are obtained from the center and the separation of the two peaks as described previously (Brutscher *et al.*, 1995). All expected 72 $H^N_i-N_i-CO_{i-1}-C^\alpha_{i-1}$ correlations (corresponding to the 76 residues minus three prolines and minus the N terminus) were unambiguously identified in the 3D MQ-HNCOCA spectrum. These "residues" were then sequentially assigned to positions in the primary peptide sequence by combined use of intraresidue $H^N_i-N_i-C^\alpha_i$ correlations as identified from the 3D HNCA experiment and sequential $H^N_i-H^N_{i+1}$ NOEs detected in the 3D $^{15}N/^{15}N$-edited NOESY experiment. In addition, $^{13}C^\alpha$ chemical shift ranges (Wishart *et al*., 1991) were used to discriminate between different amino acid types. In this way, a complete assignment of all backbone nuclei was obtained for the A state of ubiquitin, which has not been possible before using only ^{15}N-edited $^1H-^1H$ TOCSY and NOESY experiments (Stockman *et al.*, 1993).

Structural Features. In NMR studies of proteins, regular secondary structural elements are generally characterized by the presence of typical short- and medium-range NOE connectivities (Wüthrich, 1986). Strong $H^\alpha_i-H^N_{i+1}$ and small $H^N_i-H^N_{i+1}$ cross peaks are typical for β strands, whereas in the case of an α-helix the $H^N_i-H^N_{i+1}$ correlations are much stronger than the $H^\alpha_i-H^N_{i+1}$. Furthermore, the presence of $H^\alpha_i-H^N_{i+3}$ NOEs is anticipated as the distance between the two protons is ≤3.5 Å in α-helical structures. In the recorded 3D NOESY spectra the different (N_i, N_j, H^N_j) and (C^α_i, N_j, H^N_j) cross peaks are well separated and could almost completely be assigned. A summary of the identified NOE connectivity patterns is given in Figure 3. The intensities are classified as weak or strong, taking into account the different line widths in different parts of the protein (see dynamics section). The $H^N_i-H^N_j$ medium-range NOEs, given in Figure 3, show that the N-terminal part forms a nativelike two-stranded β-sheet (residues 1−7 and 11−17). Strong $H^N_i-H^N_{i+1}$ NOEs and very weak $H^\alpha_i-H^N_{i+1}$ cross peaks indicate that the rest of the protein has a predominant helical character. However, no medium-range $H^\alpha_i-H^N_{i+3}$ NOEs could be detected, probably due to the limited sensitivity of the heteronuclear filtered NOESY experiments at low sample concentration (≅0.7 mM) and large line widths (*vide infra*) as well as due to the effect of conformational averaging in this partially folded state of ubiquitin.

C^α and CO chemical shifts are useful additional indicators of secondary structural elements in proteins (Wishart *et al.*, 1991). They are only little influenced by the tertiary structure of the protein and mainly reflect local ϕ, ψ backbone torsion angles. It has been shown recently that they can be used to refine protein structures if the individual character of the different amino acids is taken into account (Le *et al.*, 1995; Pearson *et al.*, 1995). For a qualitative interpretation of the ^{13}C shifts to identify regular secondary structural elements,

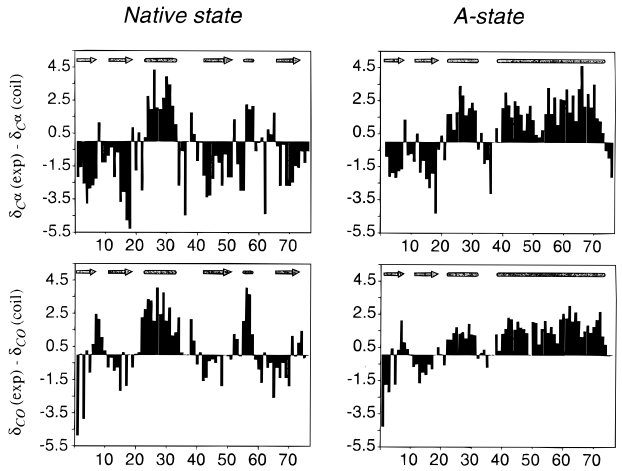

FIGURE 4: C^α and CO secondary chemical shifts of the native and the A state of ubiquitin are plotted as functions of the polypeptide sequence. The identified secondary structural elements (β-strands and α-helices) are shown on top of each graph. The assignments for the native state are taken from Wand *et al.* (1996). Amino acid type-specific random coil shifts δ_c(coil) in H_2O are taken from Richarz and Wüthrich (1978). They are not corrected for the methanol/water solvent.

it is sufficient to calculate the deviation from an amino-acid-specific random coil value (secondary chemical shift). The random coil values are obtained either by NMR measurements on model peptides (Richarz & Wüthrich, 1978) or from a statistical analysis of reported protein chemical shifts (Wishart *et al.*, 1991). In Figure 4 the C^α and CO secondary chemical shifts [calculated as deviations from the random coil values given by Richarz and Wüthrich (1978)] are plotted as a function of the peptide sequence for both the native state (Wand *et al.*, 1996; Wang *et al.*, 1995) and the A state of ubiquitin. For both sets of nuclei, the secondary shifts of the N-terminal part of the protein are very similar for the two conformations, indicating a nativelike structure in the A state. Only the absolute value of the secondary shifts is slightly reduced in the A state, which can be interpreted as conformational averaging due to a higher degree of internal dynamics. The situation is different for the C-terminal part of the protein (residues 37−72), where the chemical shift data suggest a methanol-induced transition from a mainly β-sheet structure in native ubiquitin to a state with high helicity (helix A) in the A state.

The ^{13}C differential chemical shift data can also be represented in terms of the chemical shift index (CSI) proposed by Wishart and Sykes (1994). CSI values have been calculated and included in Figure 3. Consecutive negative CSI values indicate a β-sheet structure while positive values reflect α-helical structural elements. Combining all information contained in Figure 3 leads to a *qualitative* model of the A state of ubiquitin, which is depicted in Figure 5. Three structural segments, one antiparallel β-sheet and two α-helices, are linked together without specific tertiary interactions between them. From the NMR data compiled in Figure 3, there is no evidence that the nativelike central helix B is more stable than the A-state-specific C-terminal helix A under these conditions. The two helices are connected by a linker from residues 35 to 39 with the sequence G35-I36-P37-P38-D39. The two helix-breaking prolines P37 and P38 separate these two helices. The model is in agreement with the previously reported $^1H-^{15}N$ NMR data of Stockman *et al.* (1993) and

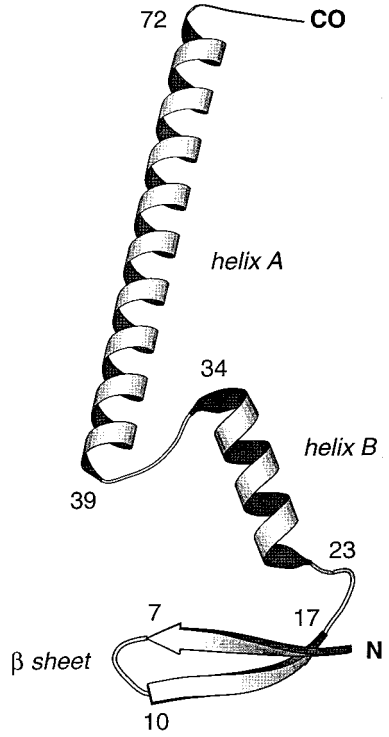

FIGURE 5: Sketch of structural model for the methanol-induced A state of ubiquitin. The presence of three loosely coupled secondary structural elements (an antiparallel β-sheet and helices A and B) is supported by the NMR data reported in this study ($^1H-^1H$ NOEs, ^{13}C secondary chemical shifts, and ^{15}N relaxation data). All three structural elements show enhanced internal mobility, as compared to native ubiquitin and most secondary structures of folded proteins. The β-sheet conformation is taken from the PDB file of the native state of ubiquitin and is consistent with the interstrand $H^N_i-H^N_j$ NOEs reported in Figure 3. The model has been drawn using the program MOLSCRIPT (Kraulis, 1991).

CD studies by Wilkinson and Mayer (1986) and Cox *et al.* (1993), indicating that the A state contains more helical structure than the native state. Conclusions drawn by other groups using 2D NMR techniques and hydrogen-exchange labeling, however, are not supported by the present study. They reported evidence of a third C-terminal β-strand (Harding *et al.*, 1991) or concluded that the general shape of the native structure is conserved but destabilized in the A state (Pan & Briggs, 1992). The latter conclusion is based on the observation of a uniform distribution of amide hydrogen protection factors along the polypeptide sequence. Protection factors are, however, less suited to discriminate between different structural models. In fact, they do not contradict our observation of helix formation in the C-terminal half. The previously reported MD simulation of ubiquitin in 60% methanol (Alonso & Daggett, 1995) did not show a transition from the β-strand to the helical state that occurs in the C-terminal half, presumably, as these authors suggest, because the lengths of the trajectories were too short (500 ps) to show the complete transition.

We would like to emphasize that the static picture given in Figure 5 is oversimplified, as the A state is highly mobile in solution. To assess the mobility, a detailed analysis of the backbone ^{15}N-relaxation behavior was carried out as is described in the following.

^{15}N Relaxation and Backbone Dynamics. ^{15}N T_1, T_2 relaxation times and $\{^1H\}^{15}N$-NOEs were measured for the A state of ubiquitin at three different NMR spectrometer

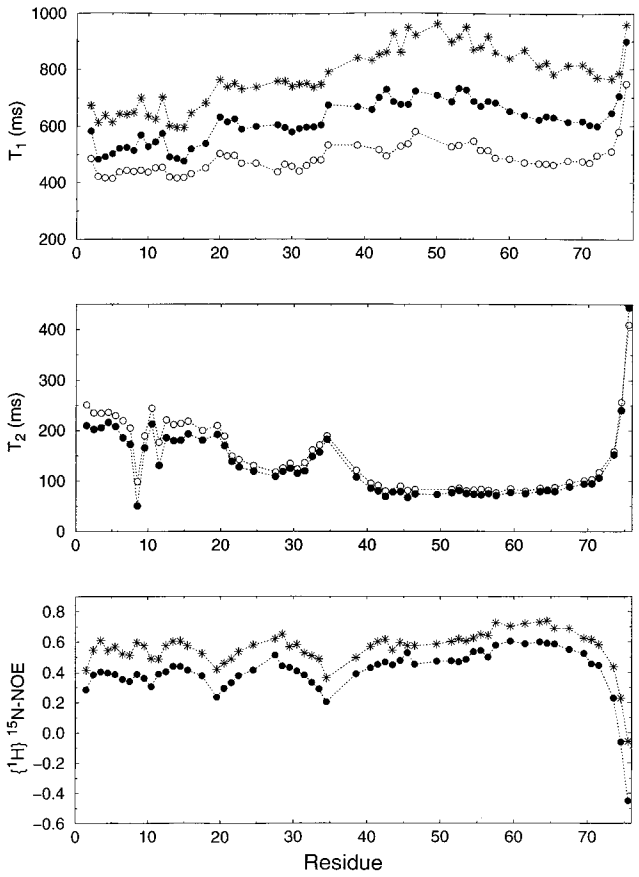

FIGURE 6: ^{15}N relaxation data (T_1, T_2, and NOE) of the A state of ubiquitin plotted as a function of the polypeptide sequence. Relaxation rates were measured at three B_0-field strengths, (○) 400 MHz, (●) 600 MHz, and (∗) 800 MHz ^{1}H frequency, at a sample temperature of 300 K.

frequencies. Due to spectral overlap in the ^{1}H−^{15}N correlation spectrum (Figure 1A), relaxation data could not be obtained for all 72 possible backbone N−H pairs (76 residues minus three prolines and the N terminal residue): relaxation parameters were extracted for 57 residues at 600 MHz (T_1, T_2, NOE) and 800 MHz (T_1, NOE) and for 53 residues at 400 MHz (T_1, T_2). The relaxation data at all three magnetic field strengths are shown in Figure 6 and they are listed in the supporting information. The qualitative patterns seen for the individual relaxation rate constants at the different field strengths are similar. Generally, the T_1 and T_2 relaxation times and the NOEs show the expected B_0-field dependence for a molecule tumbling in solution with restricted internal mobility: T_1 and NOE increase, whereas T_2 decreases with increasing magnetic B_0-field strength. Errors in the experimental data were estimated from the standard deviations of multiple measurements at 600 MHz and are in the range (4 ± 2)% (T_1), (9 ± 4)% (T_2), and (7 ± 4)% (NOE). Duplicate recordings of NOE spectra at 800 MHz yield a relative error of (2 ± 1)%.

Spin relaxation of the backbone ^{15}N nuclei is determined by the power spectral density function $J(\omega)$ that is dominated by the dipolar interaction with the directly attached proton and by the ^{15}N chemical shielding anisotropy (CSA) interaction according to

$$NOE = 1 + \frac{\gamma_H}{\gamma_N}\frac{K^2}{20}\{6J(\omega_H + \omega_N) - J(\omega_H - \omega_N)\}T_1 \quad (5)$$

$$\frac{1}{T_1} = \frac{K^2}{20}\{J(\omega_H - \omega_N) + 3J(\omega_N) + 6J(\omega_H + \omega_N)\} + \frac{C^2}{15}J(\omega_N) \quad (3)$$

$$\frac{1}{T_2} = \frac{K^2}{40}\{4J(0) + J(\omega_H - \omega_N) + 3J(\omega_N) + 6J(\omega_H) + 6J(\omega_H + \omega_N)\} + \frac{C^2}{90}\{4J(0) + 3J(\omega_N)\} + R_{ex} \quad (4)$$

with the constants $K = (\mu_0/4\pi)\gamma_N\gamma_H(h/2\pi)\langle r_{NH}^{-3}\rangle$ and $C = \omega_N(\sigma_\parallel - \sigma_\perp)$. μ_0 is the permeability of free space, γ_N and γ_H are the gyromagnetic ratios of the ^{15}N and ^{1}H nuclei, h is Planck's constant, and r_{NH} is the internuclear distance set to 1.02 Å. The CSA tensor is approximately axially symmetric with the symmetry axis parallel to the N−H bond vector. Recent liquid-state NMR studies by Bax and co-workers (Tjandra *et al.*, 1996a,b) indicate that the ^{15}N CSA tensor in proteins is nearly invariant to structural changes ($\sigma_\parallel - \sigma_\perp$) ≅ −170 ppm. The additional term R_{ex} takes into account conformational exchange contributions to T_2 resulting from processes in the micro- to millsecond time-scale range.

The power spectral density function $J(\omega)$ is defined as the Fourier transform of the autocorrelation function $C(t)$:

$$J(\omega) = \int_{-\infty}^{\infty} C(t)\exp(-i\omega t)\,dt \quad (6)$$

We assume for the autocorrelation function $C_k(t)$ of the N−H bond vector of residue k:

$$C_k(t) = e^{-|t|/\tau_{c,k}}\{S_k^2 + \sum_{j=1}^{M} A_{j,k}e^{-|t|/\tau_{j,k}}\}$$
$$\text{with} \quad S_k^2 + \sum_{j=1}^{M} A_{j,k} = 1 \quad \text{and} \quad S_k^2, A_{j,k}, \tau_{j,k} \geq 0 \quad (7)$$

$\tau_{c,k}$ represents an effective overall tumbling correlation time that is largely uncorrelated with the local internal motions and is determined by the motion of the secondary structural elements and the molecular tumbling. In the case of relatively small anisotropic reorientational motion, the overall correlation functions are in good approximation monoexponential with correlation times $\tau_{c,k}$ depending on the orientation of the N−H bond vector with respect to the principal axes of the diffusion tensor (Woessner, 1962; Brüschweiler *et al.*, 1995). In the case of a large anisotropy of the reorientational diffusion tensor, the overall tumbling contribution to $C_k(t)$ can be represented by an effective time $\tau_{c,k}$ only for special N−H bond orientations with respect to the diffusion tensor principal axes. For general N−H bond orientations, however, the overall tumbling part itself becomes multiexponential. It should be noted that, on the basis of heteronuclear NMR relaxation measurements of the type described here, it is *a priori* impossible to distinguish between local and overall motion. An interpretation of the measured correlation times is invariably bound to be subjective.

The intramolecular part of the correlation function is represented by a multiexponential function with M exponentials $A_{j,k}\exp(-|t|/\tau_{j,k})$, where $\tau_{j,k}$ is a characteristic correlation time and $A_{j,k}$ is a spatial motional coefficient. The plateau value S_k^2 is the generalized order parameter (Lipari

& Szabo, 1982 a,b) describing the motional restriction of the intramolecular motion. The motional parameters $\tau_{c,k}$, $\{\tau_{j,k}\}$, $\{A_{j,k}\}$ were determined for each residue by least-squares fitting to the relaxation data. For simplicity, the index k will be omitted in the following discussion.

For isotropic molecular tumbling, it is known that the T_2/T_1 ratio is determined exclusively by the overall rotational correlation time τ_c under the assumption that exchange processes do not contribute to transverse relaxation ($R_{ex} \cong 0$) and that internal motions are fast compared to the inverse of the involved Larmor frequencies ($\omega_0\tau_j \ll 1$) (Kay *et al.*, 1989). Figure 7 shows the T_2/T_1 ratios measured at 600 MHz for the native and the A state of ubiquitin. In the case of the native state, most of the residues show ratios around 0.37, which correspond to a rotational correlation time of 4.1 ns. In the case of the A state, on the other hand, the T_2/T_1 ratios vary between 0.15 and 0.45, implying a high degree of differential mobility along the polypeptide chain. From Figure 7, one can identify three polypeptide segments of different mobility, which coincide well with the secondary structural segments of the A state that emerged from the CO, C^α secondary chemical shifts and sequential $^1H-^1H$ NOEs (see Figures 3 and 4). Thus, the motional picture provided by the ^{15}N relaxation data is in agreement with the model in Figure 5. The three segments exhibit different average correlation times τ_c with the N-terminal β-sheet having the shortest τ_c and the C-terminal helix having the longest one. In this respect, the interpretation of the A-state dynamics somewhat resembles the description of a multidomain zinc-finger protein (Brüschweiler *et al.*, 1995), where the different domains were characterized by individual anisotropic rotational diffusion tensors.

Both helices of the A state show fraying effects in the sense that the effective τ_c values, reflected in the individual T_2/T_1 ratios, decrease and the internal mobility increases toward the ends of the helices. Such effects are neither observed for the central helix in native ubiquitin (Figure 7) nor are they characteristic for helices in other native proteins. As noted previously (Brüschweiler, 1995), such fraying effects do not necessarily reflect larger backbone dihedral angle fluctuations toward the ends of the helix but can also be the result of cumulative local motion along the whole chain (long-range motion).

The variation between the effective tumbling correlation times of the three segments and the fraying behavior indicates that the helices are stabilized by intrasegmental interactions rather than by specific tertiary interactions between the different segments, since the latter would lead to more nativelike dynamics. The large effective tumbling correlation times τ_c found for the N−H vectors in helix A could be caused by anisotropic rotational motion. For an isolated elongated helix with backbone N−H vectors that are on average parallel to the helix axis, the fast rotational diffusion about the helix axis will not modulate the N−H dipolar interaction and is thus not relaxation-active. The N−H vectors will then exhibit a correlation function with a monoexponential tumbling part with a τ_c value that is determined by the slower motions about axes perpendicular to the helix axis. Cox *et al.* (1993) studied two peptides U-21 and U-35, consisting of the first 21 and the first 35 amino acids of ubiquitin, respectively, under the A-state condition by ^1H NMR and CD. They concluded that the structure of U-35 in 60% methanol is essentially the same

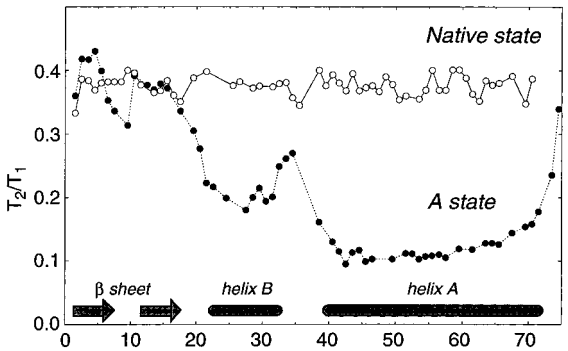

FIGURE 7: T_2/T_1 ratios calculated from the 600 MHz ^{15}N relaxation data for the native state and the A state of ubiquitin. ^{15}N relaxation rates of the native state were measured on a sample of 2 mM $^{13}C,^{15}N$-labeled ubiquitin, pH = 4.7, T = 300 K (S. Lienin and B. Brutscher, unpublished results). Not drawn are the T_2/T_1 ratios for residues T9 and T12 of the A state, which show significant conformational exchange contributions to $1/T_2$, and the unstructured C-terminal residues of the native state. Secondary structural elements as identified for the A state of ubiquitin are plotted at the bottom.

as in the intact A state and that the N-terminal β-sheet and the central helix do not strongly interact with each other. The presented ^{15}N relaxation results suggest that the latter conclusion applies for all three segments of the A state. The rather high τ_c values, on the other hand, appear to be related to the covalent connection of the three segments.

The presence of an equilibrium between the monomeric protein and aggregated states could also affect the ^{15}N relaxation data (Fushman *et al.*, 1997). To minimize such effects, samples with a low protein concentration (0.7 mM) were used for the measurements. In addition, the relevance of aggregation for the interpretation of NMR relaxation data was tested in two ways: (1) ^{15}N T_1 relaxation data were recorded for a sample with reduced concentration (0.3 mM), which does not show significant differences from the standard samples (0.7 mM). (2) An *intermolecular* $^1H-^1H$ NOESY spectrum was recorded on an A-state sample containing 50% natural abundance ubiquitin and 50% fully $^{13}C,^{15}N$-labeled ubiquitin. While no *intermolecular* cross peaks could be detected between unlabeled and labeled ubiquitin, a large number of *intramolecular* NOEs are observed. Two-dimensional inter- and intramolecular NOESY spectra are shown in the supporting information. These results indicate that the ^{15}N relaxation data reflect monomeric states. The same conclusion was reached by Cox *et al.* (1993), who studied the A state by CD, finding no evidence for aggregation over a concentration range of 0.01−5 mg/mL, which includes the sample concentration of the present study.

Each of the three protein segments shows a characteristic T_2 behavior with fraying effects toward the ends. Conformational exchange contributions R_{ex} are clearly manifested only for residues T9 and T12 located in the loop region of the β-sheet and at the beginning of the second strand of the β-sheet, respectively. For these residues the T_2 values are more than 2 standard deviations smaller than that for the neighboring residues. This picture is independently confirmed by CSA-dipole cross-correlation rate constants using the experimental scheme proposed by Tjandra *et al.*, 1996b. These parameters depend on the backbone N−H power spectral density function in a similar way as standard T_2 parameters, except that conformational exchange does not

Table 1: Extended Model-Free Analysis of ^{15}N Relaxation Data Based on Equation 7[a]

model[b]	S^2	τ_c (ns)	A_1	τ_1 (ps)	A_2	τ_2 (ps)	χ^2
			β-Sheet				
1	0.55 ± 0.08	6.0 ± 2.5	0.45 ± 0.08	720 ± 540			20.6 ± 10.6
2	0.49 ± 0.06	4.7 ± 0.8	0.34 ± 0.09	920 ± 30	0.17 ± 0.04	2.0	4.8 ± 2.3
3	0.35 ± 0.05	6.4 ± 0.9	0.44 ± 0.05	1660 ± 270	0.21 ± 0.04	41 ± 19	2.4 ± 1.2
			Helix B				
1	0.64 ± 0.03	9.1 ± 0.5	0.36 ± 0.03	920 ± 150			19.6 ± 13.2
2	0.55 ± 0.04	8.2 ± 1.0	0.34 ± 0.03	960 ± 190	0.11 ± 0.04	2.0	5.1 ± 2.5
3	0.47 ± 0.07	9.43 ± 0.6	0.36 ± 0.03	1400 ± 150	0.17 ± 0.06	42 ± 16	1.7 ± 0.7
			Helix A				
1	0.72 ± 0.03	12.2 ± 1.0	0.28 ± 0.03	1160 ± 210			7.6 ± 5.5
2	0.65 ± 0.05	12.4 ± 1.3	0.30 ± 0.03	1260 ± 240	0.05 ± 0.03	2.0	5.0 ± 4.1
3	0.58 ± 0.08	13.7 ± 1.6	0.31 ± 0.03	1830 ± 460	0.11 ± 0.06	40 ± 18	2.2 ± 1.2

[a] Values ± standard deviations of the model-free parameters averaged over the residues of the indicated segment of the ubiquitin A state, calculated for models 1, 2, and 3. [b] Fit parameters of model 1: τ_c, A_1, τ_1. Fit parameters of model 2: τ_c, A_1, τ_1, A_2. Fit parameters of model 3: τ_c, A_1, τ_1, A_2, τ_2.

contribute in this case. Experimental cross-correlation rate constants of the A state as a function of the residue number are given in the supporting information. Such a comparison represents a generally applicable method for the identification of exchange processes that overcomes ambiguities in the interpretation of T_2 data. A more quantitative analysis of the involved time constants of such exchange processes could be obtained by $T_{1\rho}$ measurements with variable spin-lock field strengths (Deverell *et al.*, 1970; Akke & Palmer, 1996).

In the following section, the question of the of multiple-time-scale internal motions will be addressed by a simultaneous fitting of all ^{15}N relaxation parameters for each residue (except for T9 and T12) assuming a correlation function of the form given in eq 7.

Extended Model-Free Analysis. The seven backbone ^{15}N-relaxation parameters, P_n^{exp}, measured for each residue ($1/T_1$ at 400, 600, and 800 MHz, $1/T_2$ at 400 and 600 MHz, and NOE at 600 and 800 MHz), were fitted by minimization of the residue-specific target function

$$\chi^2 = \sum_n \frac{(P_n^{exp} - P_n^{calc})^2}{\Delta P_n^2} \qquad (n = 1, ..., 7) \qquad (8)$$

where P_n^{calc} is the relaxation parameter P_n defined by the eqs 3−7. An effective overall rotational correlation time τ_c, which describes the average tumbling motion of the corresponding N−H vector, was fitted individually for each residue.

The data were analyzed with three different models that are all based on eq 7. In the simplest model it is assumed that the internal motion is described by a generalized order parameter S^2 and a single internal correlation time τ_1 (model 1). The extended models 2 and 3 account for the presence of two time scales of internal motion by adding a second exponential with parameters A_2 and τ_2 to the internal part of the correlation function of eq 7. In model 2 the second internal correlation time τ_2 is assumed to be very short and set to a constant value of 2.0 ps. In model 3 no restriction is applied to τ_2.

Table 1 summarizes the results of nonlinear least-squares fits of the experimental relaxation data using models 1, 2, and 3. The fitted correlation times and order parameters and the goodness of fit values χ^2 are averaged within each of the three secondary structure elements: the antiparallel β-sheet (residues 2−17), the helix B (residues 22−35) and the helix A (residues 39−72). Some features are common to all three models 1, 2, and 3:

(a) The generalized order parameters are unusually low as compared to ^{15}N relaxation studies of globular proteins where the ^{15}N order parameters for regular secondary structural elements typically lie in the range $0.80 \leq S^2 \leq 0.85$. In the A state of ubiquitin, on the other hand, most of the S^2 values lie between 0.4 and 0.6.

(b) The distinction between three separate secondary structural units, identified from ^{1}H−^{1}H NOE and ^{13}C chemical shift data, is reflected in the effective overall correlation times τ_c, which are remarkably different for the three protein segments. The lowest τ_c values are found for the N-terminal β-sheet (4.5−6.5 ns) and the highest values for the C-terminal helix A (12−14 ns). The correlation times for the short central helix B vary between 8 and 9.4 ns. This indicates that the three segments are linked flexibly and that the segmental motion is mainly determined by the concerted overall tumbling motion of the nuclei within one structural segment.

(c) Internal motions on a nanosecond time scale take place in all three structural segments of the A state of ubiquitin, in agreement with observations made on other partially denatured proteins by NMR relaxation measurements.

The χ^2 values are reduced by a factor of 2−4 when passing from model 1 to model 2, indicating that the simple model assuming only one effective internal correlation time is insufficient to describe the dynamics of this mobile protein state. We should emphasize that only the B_0-field dependence of the ^{15}N relaxation data allows one to address multiple-time scale motions, as the ^{15}N T_1, T_2, and NOE values obtained at 600 MHz B_0-field strength can be fitted perfectly using the simple model 1. A further slight decrease of χ^2 is obtained by adjusting also the internal correlation time τ_2 (model 3). Figure 8 shows the residue-specific overall and internal correlation times and order parameters obtained with model 3.

The three structural segments of the protein show similar internal mobility. The two time scales of internal motion are more than 1 order of magnitude apart, one of them representing the fast local fluctuations (thermal vibrations and librational modes) in the $\tau_2 = 1-60$ ps range and coefficients A_2 ranging between 0.1 and 0.2. This behavior is similar to the one found in globular proteins. The longer

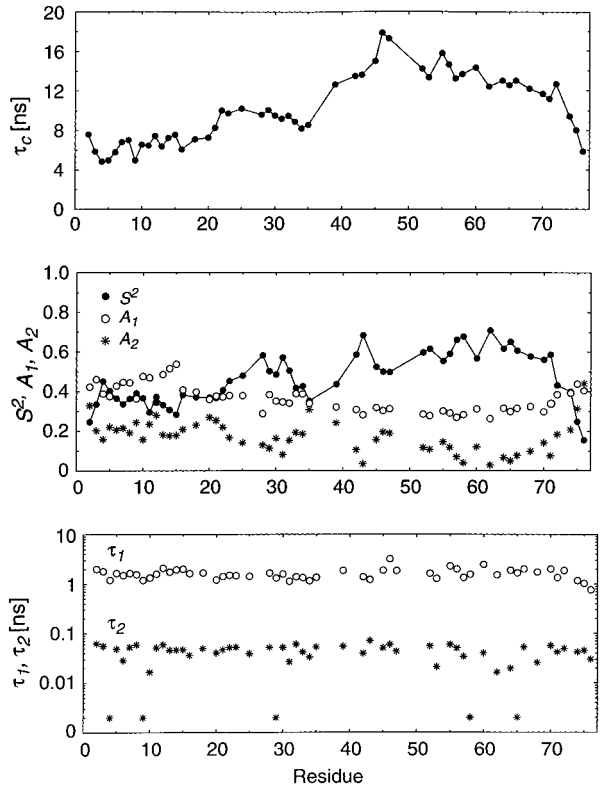

FIGURE 8: Residue-specific correlation times and order parameters obtained from a nonlinear least-squares fit to the seven experimental relaxation parameters of Figure 6 using eq 7 with two different correlation times of internal motion. The fit parameters for each residue in the model are the overall correlation time τ_c, a generalized order parameter S^2, and two effective correlation times τ_1 and τ_2, describing internal motions with contributions A_1 and A_2, respectively. The internal correlation times τ_1 and τ_2 are plotted on a logarithmic scale.

internal correlation time τ_1 describes internal motions in the range between 1 and 3 ns with relatively high coefficients A_1 ranging between 0.3 and 0.5 that are rarely observed in native proteins. The inclusion of a second internal correlation time is accompanied by an increase in the overall correlation times τ_c and a decrease in the generalized order parameters S^2. Thus, the neglect of multiple internal time scales (model 1) may underestimate the rotational correlation time and overestimate the generalized order parameter. The flexible character of the three segments inferred by the ^{15}N relaxation data is in agreement with the results obtained from the secondary chemical shifts and ^{1}H$-^1$H NOEs.

While the faster of the two time scales τ_2 lying in the picosecond range undoubtedly reflects internal motion, some ambiguity remains concerning the interpretation of motion taking place on the slower time scales τ_1. In the preceding analysis based on eq 7, the slow motion was assumed to correspond also to internal motion, which would also explain the averaging effects observed for secondary chemical shifts and ^{1}H$-^1$H NOEs. Alternatively, the main origin of the τ_1 time-scale effects could be strong tumbling anisotropy for the molecular fragments as mentioned above. The internal motions responsible for averaging the secondary chemical shifts and the ^{1}H$-^1$H NOEs would then have to occur on time scales slower than the deduced value of τ_c but faster than milliseconds, since no exchange broadening is observed for all but a few residues. On the basis of the present data, we cannot rule out this second interpretation.

This study reveals similarities to as well as differences from previous NMR investigations of partially folded protein states. The N-terminal part of the immunoglobulin binding domain of streptococcal protein G (GB1) forms in the native state an antiparallel β-sheet (residues 1−20) and an α-helix (residues 22−37) similar to native ubiquitin. The urea-denatured state of GB1 at pH 2 (Frank *et al.*, 1995) does not show any residual secondary structure, which is comparable to NMR results on the guanidine-hydrochloride-denatured state of ubiquitin (Briggs & Roder, 1992). With the exception of the N- and C-termini, the backbone ^{15}N order parameters are uniformly distributed between 0.4 and 0.5 with internal correlation times below 200 ps and some residues showing conformational exchange contributions. The effective tumbling correlation time is about 3 ns, which is much shorter than the one found for the ubiquitin A state, indicating a lack of segmental motion in this state of GB1. It would be interesting to investigate GB1 in an alcohol/water mixture to gain more insight in the stability of the different structural segments under "softer" denaturing conditions.

In the case of partially folded states of proteins containing cysteine residues, as reported for BPTI (van Mierlo *et al.*, 1993) and interleukin 4 (Redfield *et al.*, 1994), a molten globule state is stabilized by one (BPTI) or three (interleukin 4) disulfide bonds, respectively. The highly ordered hydrophobic core of these partially folded proteins is characterized by order parameters similar to the ones found in regular secondary structural elements of native proteins ($0.7 \leq S^2 \leq 0.85$). Conversely, the low order parameters of the ubiquitin A state suggest the absence of formation of a hydrophobic core involving the three structural segments.

For hen egg white lysozyme (Buck *et al.*, 1995) and α-lactalbumin (Alexandrescu *et al.*, 1994a), partially unfolded in 70% and 50% trifluoroethanol (TFE), respectively, similar observations are made as for the A state of ubiquitin: some of the native structure is retained and additional nonnative helical structure is induced with strongly reduced tertiary interactions. While in the TFE state of hen egg white lysozyme the order parameters are strongly affected by their sequence position relative to the nearest disulfide bridge, many of the internal correlation times lie in the low nanosecond range (Buck *et al.*, 1996) similar to the A state of ubiquitin.

Alcohols appear to denature native states of proteins by disrupting the (noncovalent) tertiary interactions, presumably by weakening the hydrophobic effect relative to hydrogen-bonding interactions (Nelson & Kallenbach, 1986). Future NMR studies on denatured protein states will further improve the understanding of the local interactions responsible for the formation of native and nonnative structure as well as the conformational flexibility, which are essential factors contributing to the *in vivo* activity of these biomolecules.

CONCLUSION

This study demonstrates that the partial unfolding of a protein by solvent interactions not only leads to enhanced local mobility but also can induce altered secondary structural elements. The N-terminal half retains the structural features of the native β-sheet and of the central helix B but shows significantly increased internal mobility. In the C-terminal half, methanol induces a transition from the native β-strand-

rich region to an elongated segment with high helical propensity (helix A). These segments were identified on the basis of characteristic CO and C^{α} secondary chemical shifts, $^1H-^1H$ NOE connectivities, and CD data, and they coincide well with the segments found in the ^{15}N relaxation data. All three segments are involved in dynamic equilibria between flexible structural elements as is reflected by the ^{15}N backbone order parameters, by the secondary chemical shifts, and by the absence of $H^{\alpha}_i-H^N_{i+3}$ NOEs in both helical segments A and B. The ^{15}N relaxation data measured at three magnetic field strengths reveal enhanced multiple-time-scale backbone mobilities, which markedly differ from the dynamics of the native state. This structural and dynamical picture of the A state of ubiquitin represents a phenotype of partially unfolded proteins, which is characterized by a combination of native and nonnative secondary structural elements with high internal mobility, connected by flexible linkers.

ACKNOWLEDGMENT

We thank Professor A. J. Wand for providing $^{13}C,^{15}N$-labeled ubiquitin, M. Schick for helpful discussions, and Professor C. Griesinger and Dr. H. Schwalbe for spectrometer time and assistance on the Bruker NMR spectrometer DMX-800 at the University of Frankfurt.

SUPPORTING INFORMATION AVAILABLE

Two tables, containing the H^N, N, CO, and C^{α} chemical shift assignments of the methanol-induced A state of ubiquitin and the ^{15}N relaxation data (T_1, T_2, NOE) of ubiquitin A state measured at 400, 600, and 800 MHz B_0-field strength, and five figures with pulse sequences for ^{15}N relaxation experiments (T_1, T_2, NOE) on $^{13}C,^{15}N$-labeled samples, pulse sequences and 2D spectra of the inter- and intramolecular ^1H NOESY experiments, and experimental $^{15}N-^1H$ chemical shielding anisotropy−dipolar cross-correlated rate constants for the A state of ubiquitin (11 pages). Ordering information is given on any current masthead page.

REFERENCES

Akke, M., & Palmer, A, G. (1996) *J. Am. Chem. Soc. 118*, 911−912.
Alexandrescu, A. T., & Shortle, D. (1994) *J. Mol. Biol. 242*, 527−546.
Alexandrescu, A. T., Ng, Y.-L., & Dobson, C. M. (1994a) *J. Mol. Biol. 235*, 587−599.
Alexandrescu, A. T., Abeygunawardana, C., & Shortle, D. (1994b) *Biochemistry 33*, 1063−1072.
Alonso, D. O. V., & Daggett, V. (1995) *J. Mol. Biol. 247*, 501−520.
Bax, A., & Pochapsky, S. (1992) *J. Magn. Reson. 99*, 638−643.
Bax, A., Griffey, R. H., & Hawkins, B. L. (1983) *J. Magn. Reson. 55*, 301−315.
Bodenhausen, G., & Ruben, D. J. (1980) *Chem. Phys. Lett. 69*, 185−189.
Briggs, M. S., & Roder, H. (1992) *Proc. Natl. Acad. Sci. U.S.A. 89*, 2017−2021.
Brüschweiler, R., Liao, X., & Wright, P. (1995) *Science 268*, 886−889.
Brüschweiler, R. (1995) *J. Chem. Phys. 102*, 3396−3403.
Brutscher, B., Cordier, F., Simorre, J.- P., Caffrey, M., & Marion, D. (1995) *J. Biomol. NMR 5*, 202−206.
Buck, M., Schwalbe, H., & Dobson, C. M. (1995) *Biochemistry 34*, 13219−13232.
Buck, M., Schwalbe, H., & Dobson, C. M. (1996) *J. Mol. Biol. 257*, 669−683.
Burgering, M., Boelens, R., & Kaptein, R. (1993) *J. Biomol. NMR 3*, 709−714.
Clore, G. M., Szabo, A., Bax, A., Kay, L. E., Driscoll, P. C., & Gronenborn, A. M. (1990) *J. Am. Chem. Soc. 112*, 4989−4991.
Cox, J. P. L., Evans, P. A., Packman, L. C., Williams, D. H., & Woolfson, D. N. (1993) *J. Mol. Biol. 234*, 483−492.
Deverell, C., Morgan, R. E., & Strange, J. H. (1970) *Mol. Phys. 18*, 553−559.
Di Stefano, D. L., & Wand, A. J. (1987) *Biochemistry 26*, 7272−7281.
Ecker, D. J., Butt, T. R., Marsh, J., Sternberg, E., Shatzman, A., Dixon, J. S., Weber, P. L., & Crooke, S. T. (1989) *J. Biol. Chem. 264*, 1887−1893.
Farrow, N. A., Muhandiram, R., Singer, A. U., Pascal, S. M., Kay, C. M., Gish, G., Shoelson, S. E., Pawson, T., Forman-Kay, J. D., & Kay, L. E. (1994) *Biochemistry 33*, 5984−6003.
Farrow, N., Zhang, O., Forman-Kay, J. D., & Kay, L. E. (1995) *Biochemistry 34*, 868−878.
Farrow, N., Zhang, O., Forman-Kay, J. D., & Kay, L. E. (1997) *Biochemistry 36*, 2390−2402.
Feng, Y., Sligar, S. G., & Wand, A. J. (1994) *Nat. Struct. Biol. 1*, 30−35.
Frank, M. K., Clore, G. M., Gronenborn, A. M. (1995) *Protein Sci. 4*, 2605−2615.
Fushman, D., Cahill, S., & Cowburn, D. (1997) *J. Mol. Biol. 266*, 173−194.
Grzesiek, S., & Bax, A. (1992) *J. Magn. Reson. 96*, 432−440.
Grzesiek, S., & Bax, A. (1993) *J. Am. Chem. Soc. 115*, 12593−12594.
Harding, M. M., Williams, D. H., & Woolfson, D. N. (1991) *Biochemistry 30*, 3120−3128.
Ikura, M., Kay, L. E., & Bax, A. (1990) *Biochemistry 29*, 4659−4667.
Jeener, J., Meier, B. H., Bachmann, P., & Ernst, R. R. (1979) *J. Chem. Phys. 71*, 4546−4553.
Kay, L. E., Torschia, D. A., & Bax, A. (1989) *Biochemistry 28*, 8972−8979.
Kay, L. E., Ikura, M., Tschudin, R., & Bax, A. (1990) *J. Magn. Reson. 89*, 497−514.
Kraulis, P. J. (1991) *J. Appl. Crystallogr. 24*, 946−950.
Le, H., Pearson, J. G., de Dios, A., & Oldfield, E. (1995) *J. Am. Chem. Soc. 117*, 3800−3807.
Lipari, G., & Szabo, A. (1982a) *J. Am. Chem. Soc. 104*, 4546−4559.
Lipari, G., & Szabo, A. (1982b) *J. Am. Chem. Soc. 104*, 4559−4570.
Logan, T. M., Thériault, Y., & Fesik, S. (1994) *J. Mol. Biol. 236*, 637−648.
Marion, D., Ikura, M., Tschudin, R., & Bax, A. (1989) *J. Magn. Reson. 85*, 393−399.
Montelione, G. T., & Wagner, G. (1990) *J. Magn. Reson. 87*, 183−188.
Nelson, J. W., & Kallenbach, N. R. (1986) *Proteins: Struct., Funct., Genet. 1*, 211−217.
Neri, D., Billeter, M., Wider, G., & Wüthrich, K. (1992) *Science 257*, 1559−1563.
Pan, Y., & Briggs, M. (1992) *Biochemistry 31*, 11405−11412.
Pearson, J. G., Wang, J.-F., Markley, J., Le, H., & Oldfield, E. (1995) *J. Am. Chem. Soc. 117*, 8823−8829.
Peng. J. W., & Wagner, G. (1992) *J. Magn. Reson.. 98*, 308−332.
Rechsteiner, M., Ed. (1988) *Ubiquitin*, Plenum Press, New York.
Redfield, C., Smith, R. A. G., & Dobson, C. M. (1994) *Nat. Struct. Biol. 1*, 23−29.
Richarz, R., & Wüthrich, K. (1978) *Biopolymers 17*, 2133−2141.
Schneider, D. M., Dellwo, M. J., & Wand, J. A. (1992) *Biochemistry 31*, 3645−3652.
Skelton, N. J., Palmer, A. G., Akke, M., Kördel, J., Rance, M., & Chazin, W. (1993) *J. Magn. Reson., Ser. B 102*, 253−264.
Sklenar, V., Piotto, M., Leppik, R., & Saudek, V. (1993) *J. Magn. Reson. 102*, 241−245.
Stockman, B., Euvrard, A., & Scahill, T. A. (1993) *J. Biomol. NMR 3*, 285−296.
Tjandra, N., Feller, S. E., Pastor, R. W., & Bax, A. (1995) *J. Am. Chem. Soc. 117*, 12562−12566.
Tjandra, N., Wingfield, P., Stahl, S., & Bax, A. (1996a) *J. Biomol. NMR 8*, 273−284.
Tjandra, N., Szabo, A., & Bax, A. (1996b) *J. Am. Chem. Soc. 118*, 6986−6991.

Tycko, R., Ed. (1994) *Nuclear Magnetic Resonance Probes of Molecular Dynamics*, Kluwer, Dordrecht, The Netherlands.
van Mierlo, C. P. M., Darby, N. J., Keeler, J., Neuhaus, D., & Creighton, T. E. (1993) *J. Mol. Biol. 229*, 1125−1146.
Vijay-Kumar, S., Bugg, C. E., & Cook, W. J. (1987) *J. Mol. Biol. 194*, 531−544.
Wand, A. J., Urbauer, J. L., McEvoy, R. P., & Bieber, R. J. (1996) *Biochemistry 35*, 6116−6125.
Wang, A. C., Grzesiek, S., Tschudin, R., Lodi, P. J., & Bax, A. (1995) *J. Biomol. NMR 5, 376−382.*
Weber, P. L., Brown, S. C., & Mueller, L. (1987) *Biochemistry 26*, 7282−7290.
Wilkinson, K. D., & Mayer, A. N. (1986) *Arch. Biochem. Biophys. 250*, 390−399.
Wishart, D. S., & Sykes, B. D. (1994) *J. Biomol. NMR 4*, 171−180.
Wishart, D. S., Sykes, B. D., & Richards, F. M. (1991) *J. Mol. Biol. 222*, 311−333.
Woessner, D. E. (1962) *J. Chem. Phys. 37*, 647−654.
Woolfson, Harding, M. M., Evans, P. A., & Williams, D. H. (1991) *Techniques in Protein Chemistry II*, pp 283−293, Academic Press, San Diego.
Woolfson, D. N., Cooper, A., Harding, M. M., Williams, D. H., & Evans, P. A. (1993) *J. Mol. Biol. 229*, 502−511.
Wüthrich, K. (1986) *NMR of Proteins and Nucleic Acids*, John Wiley & Sons, New York.

BI971538T